Korean J. Chem. Eng., 33(5), 1640-1646 (2016)
DOI: 10.1007/s11814-016-0012-y

pISSN: 0256-1115
eISSN: 1975-7220

Synthesis of magnetic $Co_{1-x}Ni_xFe_2O_4$/carbon nanotubes with controlled microstructure for adsorption of pentachlorophenol

Chunyue Cui†, Mengyuan Sun, and Qingzhu Zheng

Qingdao Engineering Research Center for Rural Environment, Qingdao Agricultural University, Qingdao 266109, China
(*Received 10 September 2015 • accepted 11 January 2016*)

Abstract−Magnetic $Co_{1-x}Ni_xFe_2O_4$/Carbon nanotube (CNTs) nanocomposite was successfully prepared by hydrothermal method and used for the adsorption of pentachlorophenol. The properties of $Co_{1-x}N_xFe_2O_4$/CNTs were characterized by scanning and transmission electron microscopy, energy dispersive X-ray spectroscopy, X-ray diffractometry, Brunauer-Emmett-Teller surface area determination, and magnetic measurement. Results showed that the $Co_{1-x}Ni_xFe_2O_4$ nanoparticles with amorphous structure are dispersed uniformly on the CNTs, which enhanced the adsorption capacity. The $Co_{1-x}Ni_xFe_2O_4$/CNTs as a magnetic material are easy to separate from the aqueous solution in magnetic field. The adsorption capacity and magnetization were improved by controlling the Ni content and calcination temperature. In addition, the $Co_{1-x}Ni_xFe_2O_4$/CNTs loaded with pentachlorophenol (PCP) could be regenerated by microwave radiation and the regeneration efficiency reached 110% after six regeneration cycles.

Keywords: Carbon Nanotubes $Co_{1-x}Ni_xFe_2O_4$, Adsorption, Regeneration

INTRODUCTION

Chlorophenols (CPs) are listed as priority pollutant by the United States Environmental Protection Agency and have been used extensively worldwide as bactericides, insecticides, herbicides, and wood preservatives [1]. These compounds are strongly resistant to chemical, physical or biological degradation. Therefore, a rapid and safe technology for the effective treatment of CPs is urgently needed to facilitate this remediation [2].

Many kinds of technologies such as biological treatment [3], adsorption [4], and chemical treatments [5,6] have been developed and applied worldwide for the scavenging of CPs. Among these, adsorption has become one of the most powerful techniques for the removal of CP compounds because of its easy operation, low cost, high efficiency, and insensitivity to toxic pollutants [7-9].

Although activated carbon is one of the best adsorbents for the treatment of organic pollutants with higher adsorption capacity, its high cost and low regeneration ability restrict its use [10]. Therefore, the search to develop efficient adsorbents with higher adsorption and regeneration capacities is ongoing.

Carbon nanotubes (CNTs) have attracted great interest as a new type of adsorbent to remove organic pollutants from aqueous solution because of their strong hydrophobicity, large specific surface area, excellent stability, and rich surface functionalities [11-13].

However, a major drawback arises from the difficulties associated with the separation of small CNTs from aqueous solutions [14]. Serious concerns exist over the health and environmental risks of CNTs once they have been released into the environment [15]. Therefore, it is highly desirable to develop an efficient and safe technology for the collection of CNTs.

Compared with traditional centrifugation and filtration methods, magnetic separation has gradually attracted the attention of many scientists as a rapid and effective technology to separate magnetic adsorbents for environmental applications [16,17].

In recent years, CNTs have been modified with different magnetic materials and used for the removal of different pollutants in aqueous solution, which presents new opportunities for achieving desirable adsorption capacity and effective magnetic separation [18-21]. For example, Gong et al. reported that chemical coprecipitation-derived CNTs/iron oxide composites can be used as adsorbents, and exhibit good dispersibility, good magnetic properties, and excellent adsorption capacity for cationic dyes from aqueous solution [22]. Yu et al. synthesized CNTs/Fe_2O_3 adsorbent using Fenton's reagent method, and demonstrated that CNTs/Fe_2O_3 hybrids exhibit excellent magnetic, adsorption, and photocatalytic properties [23]. $CoFe_2O_4$/CNTs composites have also been prepared to remove methyl green dye from aqueous solution [24].

CNTs modified with magnetic materials show reduced adsorption ability, possibly because of the small surface area of the magnetic materials, agglomeration of the nanoparticles on the CNT surfaces, and poor interactions between the CNTs and the nanoparticles.

To determine the optimum adsorption, the effect of common parameters including pH, adsorbent dosage, and contact time has been investigated. To our knowledge, no published studies exist on the effect of the magnetic material microstructure on adsorption. Therefore, further modification is necessary to improve the adsorption and magnetic properties of CNT absorbents.

In this paper, magnetic $Co_{1-x}Ni_xFe_2O_4$/CNTs nanocomposite adsorbent was prepared by the hydrothermal method. The magnetic properties and adsorption capacity of the $Co_{1-x}Ni_xFe_2O_4$/CNTs nanocomposites can be controlled through adjusting the atomic

†To whom correspondence should be addressed.
E-mail: cuichunyue@126.com

ratios and calcination temperature. In addition, $Co_{1-x}Ni_xFe_2O_4$/CNTs adsorbent regenerated by microwave radiation.

EXPERIMENTAL

1. Preparation and Oxidation of CNTs

CNTs were prepared according to the procedure reported in our previous work [25]. The CNTs were oxidized with a 3.0 M H_2SO_4-HNO_3 (1 : 1) mixture at 100 °C for 6 h under reflux, and then washed with deionized water, filtered, and dried in vacuum for 10 h.

2. Synthesis of $Co_{1-x}Ni_xFe_2O_4$/CNTs

A hydrothermal method was used to prepare magnetic composites composed of $Co_{1-x}Ni_xFe_2O_4$. The typical preparation process (x=0.4) is described as follows: 0.300 g of treated CNTs, 0.0186 g of $Co(NO_3)_2{\cdot}6H_2O$, 0.0124 g of $Ni(NO_3)_2{\cdot}6H_2O$, 0.172 g of $Fe(NO_3)_3{\cdot}9H_2O$, and 3.6 g of NaAc were dissolved in 100 mL ethylene glycol and 1.5 mL polyethylene glycol, then ultrasonic oscillating for 1 h to achieve a uniform mixed solution. The resulting mixture was inserted into an autoclave, heated at 180 °C for 12 h. After cooling to room temperature, the product was centrifuged, washed several times with water and ethanol, and then dried under vacuum.

By varying the atomic ratio of the Co and Ni salts in the mixed nitrate solution with x=0, 0.2, 0.4, 0.5, and 0.6, respectively, a series of $Co_{1-x}Ni_xFe_2O_4$/CNTs nanocomposites were synthesized under the same conditions.

3. Adsorption and Regeneration

3-1. Adsorption Experiments

Batch adsorption experiments were conducted to study the effect of $Co_{1-x}Ni_xFe_2O_4$/CNTs on PCP adsorption at room temperature. All experiments were in duplicate. The solutions of all of the samples were adjusted to pH 7, and were filtered with 0.45 μm filter membrane. The concentration of PCP was determined by ultraviolet-visible spectrophotometer (UV-2550; Shimadzu, Japan,) at 320 nm. The absorption capacity (G_e, mg g^{-1}) was calculated from Eq. (1):

$$G_e = \frac{(c_0 - c_e)V}{m} \quad (1)$$

where C_0 and C_e are the initial and equilibrium concentrations of PCP (mg L^{-1}), m is the mass of $Co_{1-x}Ni_xFe_2O_4$/CNTs (g), and V is the solution volume (L).

3-2. Regeneration Experiments

The $Co_{1-x}Ni_xFe_2O_4$/CNTs adsorbents saturated with PCP were separated from the aqueous solution with a magnet. The collected $Co_{1-x}Ni_xFe_2O_4$/CNTs were placed into a quartz reactor and regenerated by microwave (MW) irradiation. The MW regeneration system is described in our previous work [26]. MW energy was supplied at 2,450 MHz with continuous adjustable power settings from 0 to 850 W. A quartz reactor (25 mm inner diameter) was installed in the MW oven. The top of the reactor was connected to a distillate collection system.

After regeneration, the $Co_{1-x}Ni_xFe_2O_4$/CNTs nanocomposites were rinsed with distilled water and dried under vacuum at 105 °C for 8 h. Re-adsorption experiments were performed following the procedure described above. Adsorption and regeneration were repeated for six cycles to evaluate the adsorbent reusability.

4. Analytical Methods

The morphology of CNTs and $Co_{1-x}Ni_xFe_2O_4$/CNTs was characterized by scanning electron microscopy (SEM, JEOL-7500F, Japan) and transmission electron microscopy (TEM, JEOL-2010F, 200 kV). Structural characterization of the samples was performed by X-ray diffractometry (XRD, LabxXRD-6000, Shimadzu, Japan) with Cu Ka radiation. Energy dispersive X-ray spectrometry (EDX) was used for elemental analysis. The Brunauer-Emmett-Teller (BET) surface area was analyzed by nitrogen adsorption (NOVA 1200E). Magnetic properties of the samples were characterized by vibrating sample magnetometry (BHV-525, Riken Denshi) in the field of ±5 kOe at room temperature.

RESULTS AND DISCUSSION

1. Characterization of $Co_{1-x}Ni_xFe_2O_4$/CNTs

Fig. 1(a) shows a typical SEM image of the purified CNTs. The outer diameters of CNTs have in the range of 30-50 nm, and lengths of up to several tens of micrometers. The SEM image in Fig. 1(b), shows that the magnetic nanoparticles have high dispersion on the surface of CNTs. In addition, the TEM image in Fig. 1(c) clearly shows that the nanoparticles are uniformly coated on the CNT

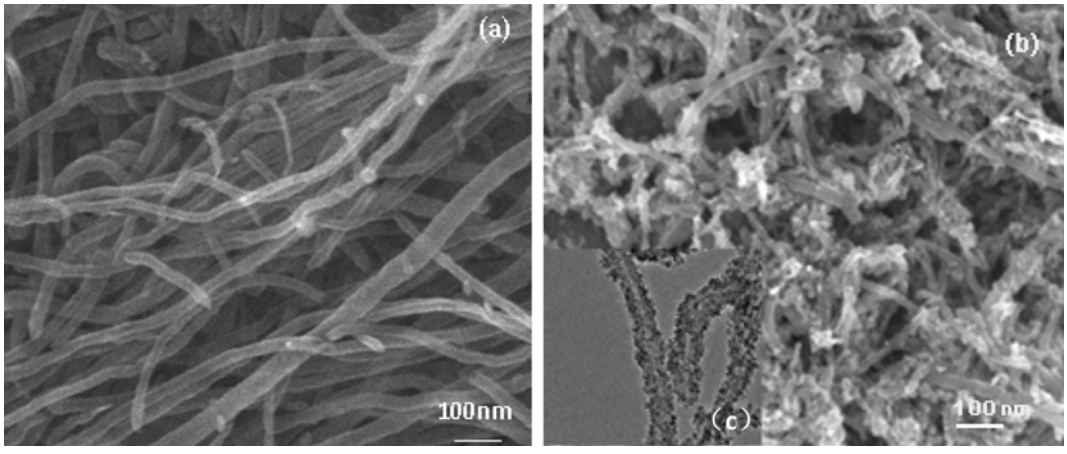

Fig. 1. SEM images of CNTs (a) and $Co_{1-x}Ni_xFe_2O_4$/CNTs (b); TEM images of $Co_{1-x}Ni_xFe_2O_4$/CNTs (c).

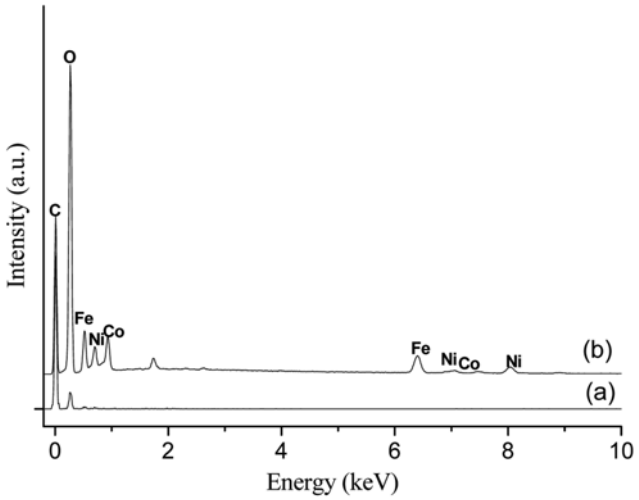

Fig. 2. EDX analyses of CNTs (a) and $Co_{1-x}Ni_xFe_2O_4$/CNTs (b).

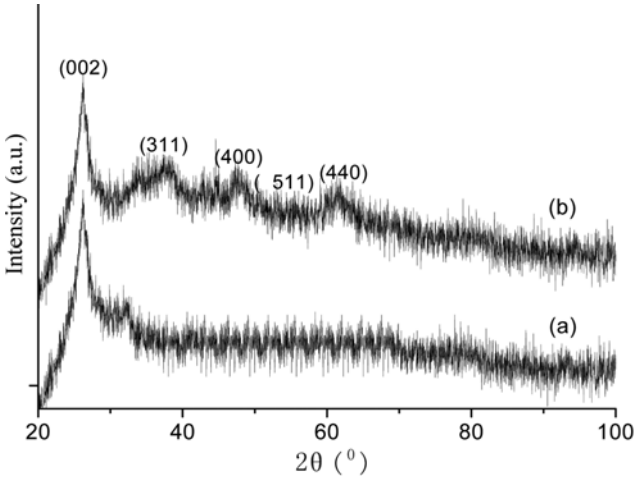

Fig. 3. XRD patterns of CNTs (a) and $Co_{1-x}Ni_xFe_2O_4$/CNTs (b).

surface with small size.

Fig. 2 shows selected area EDX spectra for CNTs and $Co_{1-x}Ni_xFe_2O_4$/CNTs. The CNTs spectra (Fig. 2(a)) are composed of elemental C and O. Compared with the spectrum in Fig. 2(a), Fig. 2(b) shows additional peaks corresponding to elemental Fe, Co, and Ni. The magnetic material and CNT mass ratio is 1 : 5.

The XRD patterns of the CNTs and $Co_{1-x}Ni_xFe_2O_4$/CNTs are shown in Fig. 3. It clearly shows the typical peak of the (002) CNT phase (Fig. 3(a)). The peaks at 35.4°, 43.2°, 57.4°, and 62.8° are attributed to the (311), (400), (511), and (440) phase of $Co_{1-x}Ni_xFe_2O_4$, respectively (Fig. 3(b)). [27]. However, the peaks of $Co_{1-x}Ni_xFe_2O_4$ are weak and broad. Therefore, it can be concluded that for the magnetic materials, the degree of crystallization is low and their structure is mainly amorphous. The amorphous structure may provide better adsorption ability than the crystal structure [28]. The BET surface areas of the CNTs and $Co_{1-x}Ni_xFe_2O_4$/CNTs were 156.7 $m^2 g^{-1}$ and 179.5 $m^2 g^{-1}$, respectively.

The magnetic properties of CNTs and $Co_{1-x}Ni_xFe_2O_4$/CNTs materials were studied at room temperature by using a vibrating sample magnetometer. Fig. 4 shows that the CNTs were not magnetic, but the hysteresis loops of the $Co_{1-x}Ni_xFe_2O_4$/CNTs samples are typical loops of a soft magnet and the saturation magnetization of the

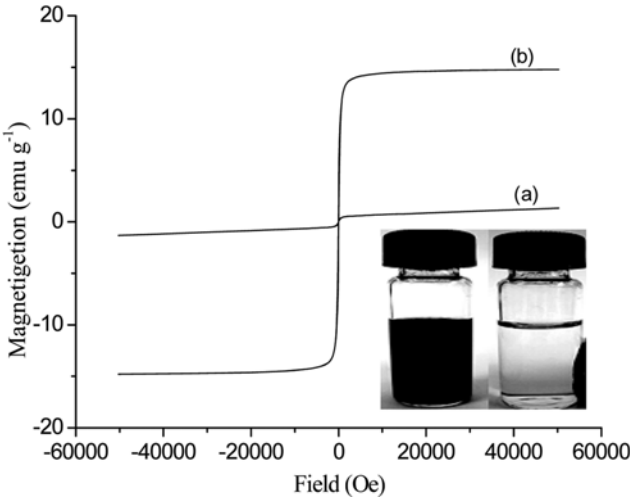

Fig. 4. Magnetic hysteresis curves for CNTs (a) and $Co_{1-x}Ni_xFe_2O_4$/CNTs (b).

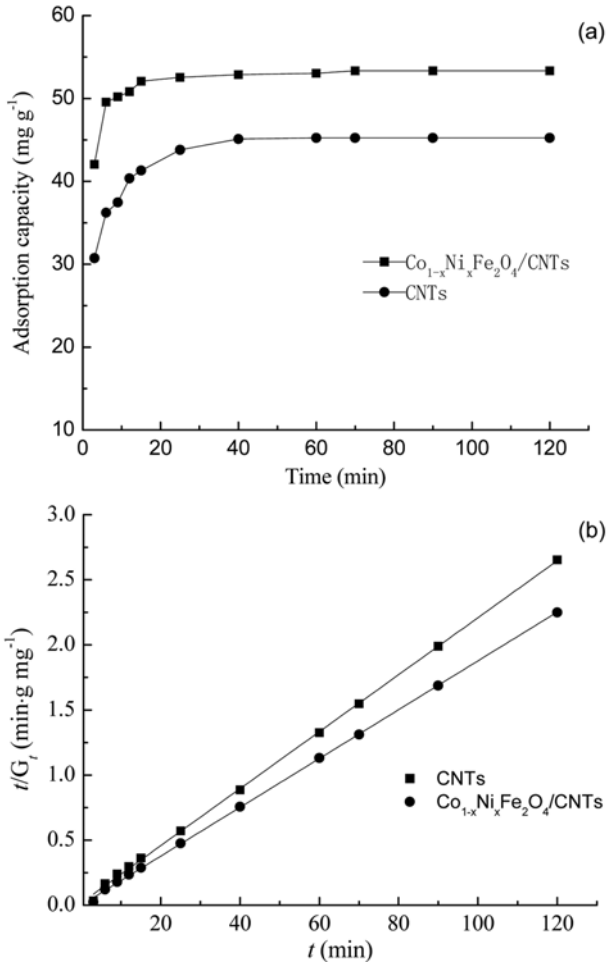

Fig. 5. Adsorption kinetics (a) and Lagergren kinetic models (b) of PCP on CNTs and $Co_{1-x}Ni_xFe_2O_4$/CNTs.

materials is 14.41 emu g^{-1}. As shown in Fig. 4, the $Co_{1-x}Ni_xFe_2O_4$/CNTs have stable dispersion ability and rapid response to an applied external magnetic field. This indicates that it is possible to collect the $Co_{1-x}Ni_xFe_2O_4$/CNTs using a magnetic field after adsorption of the organic pollutants in water.

2. Adsorption Kinetics

To evaluate the adsorptive properties of $Co_{1-x}Ni_xFe_2O_4$/CNTs, it is important to investigate the rate at which contaminants are removed from aqueous solution. Fig. 5(a) shows the effect of contact time on the amount of PCP removed by CNTs and $Co_{1-x}Ni_xFe_2O_4$/CNTs. The adsorption capacity of PCP by CNTs and $Co_{1-x}Ni_xFe_2O_4$/CNTs increased rapidly initially (during the first 25 min) and then became smooth with contact time. The rate of removal reached a plateau after approximately 60 min.

To further understand the characteristics of the adsorption process, the Lagergren kinetic model was applied to fit experimental data obtained from batch experiments [29].

$$\frac{t}{G_t} = \frac{1}{k_2 G_e^2} + \frac{1}{G_e} t \quad (2)$$

where G_e and G_t are the amount of PCP adsorbed (mg g^{-1}) at equilibrium and time t (min), respectively, and k_2 is the rate constant (min^{-1}). The rate constants of k_2 and G_e can be calculated from the intercept and slope of the line in the t/G_t versus t, respectively. Fig. 5(b) presents the adsorption kinetics of PCP on the CNTs and $Co_{1-x}Ni_xFe_2O_4$/CNTs which fitted well to the Lagergren kinetic model. From linear fitting, the correlation coefficients R were found to be greater than 0.99 and the adsorption data fitted the Lagergren kinetic model. G_e of the CNTs and $Co_{1-x}Ni_xFe_2O_4$/CNTs reached 45.68 mg g^{-1} and 53.30 mg g^{-1} and k_2 was 0.021 min^{-1} and 0.178 min^{-1}, respectively. This comparison suggests that $Co_{1-x}Ni_xFe_2O_4$/CNTs have significant potential for use as adsorbents in wastewater treatment, and show the main advantage of separation convenience.

3. Adsorption Isotherms

An adsorption isotherm is helpful in describing the distribution between the solid and liquid phase when the adsorption reaches equilibrium. Fig. 6 presents the adsorption of PCP at various initial concentrations (5-200 mg/L) in 60 min using 50 mg CNTs and $Co_{1-x}Ni_xFe_2O_4$/CNTs at pH 7 and 25 °C. The adsorption capacity increases with increasing initial concentration.

The adsorption thermodynamics of PCP on the CNTs and $Co_{1-x}Ni_xFe_2O_4$/CNTs was fitted to the Freundlich model:

$$G_e = k_F C_e^{1/n}, \quad (3)$$

where G_e (mg g^{-1}) is the equilibrium adsorption capacity, C_e (mg L^{-1}) is the equilibrium concentration of PCP in solution, and k_F and n are indicators of adsorption capacity and adsorption strength, respectively. Fig. 6 shows that the Freundlich isotherm model performs well in representing the kinetic data (R^2>0.99), which indicates that multilayer adsorption of PCP occurs onto the composite. The model parameters were determined by nonlinear regression and k_F of the CNTs and $Co_{1-x}Ni_xFe_2O_4$/CNTs was 28.57 and 35.27 and n was 6.42 and 6.55, respectively. This indicates that the Freundlich constants values n were found to be greater than 1, which is favorable for adsorption [30]. Furthermore, these results indicated that the CNTs modified with $Co_{1-x}Ni_xFe_2O_4$ exhibit improved PCP adsorption owing to the high surface area.

4. Effect of Ni Content

A partial replacement of Co^{2+} with Ni^{2+} can improve characteristics of the $CoFe_2O_4$ ferrite microstructure, such as the particle size and magnetic properties. The BET surface area and saturation mag-

Table 1. Surface structural properties of $Co_{1-x}Ni_xFe_2O_4$/CNTs at different Ni content (x)

x	BET surface area/ (m^2 g^{-1})	Saturation magnetization/ (emu g^{-1})
0	159.1	19.03
0.2	162.9	16.82
0.4	179.5	14.41
0.5	172.9	12.35
0.6	165.5	11.06

Note: ($mCo_{1-x}Ni_x$:m Fe_2O_4 is 1 : 5)

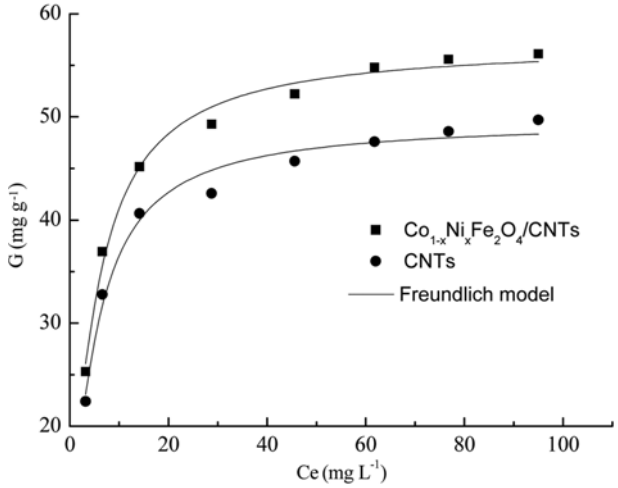

Fig. 6. Adsorption isotherm of PCP on CNTs and $Co_{1-x}Ni_xFe_2O_4$/CNTs following the Freundlich model.

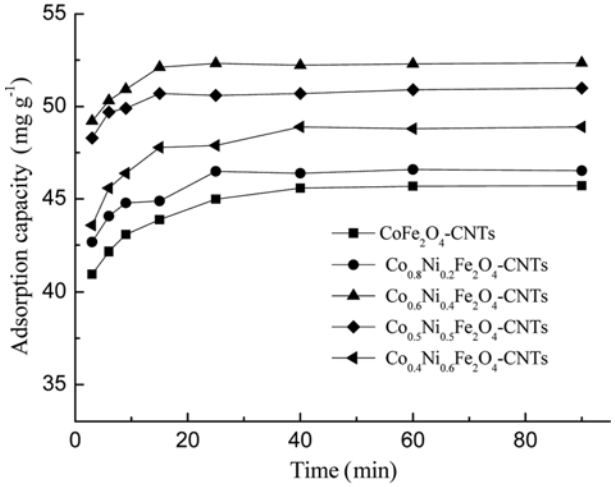

Fig. 7. Effect of Ni content on PCP adsorption.

netization of $Co_{1-x}Ni_xFe_2O_4$/CNTs with different Ni content are shown in Table 1. As shown in Table 1, the saturation magnetization decreases with increasing Ni content. The BET surface area increases the Ni content for Ni content (x) from 0 to 0.4 and shows a significant decrease with increasing Ni content for *x* from 0.4 to 0.6.

Results for adsorption of PCP by $Co_{1-x}Ni_xFe_2O_4$ at different Ni content (0<x<0.6) are shown in Fig. 7. When x ranges from 0 to 0.4, the PCP adsorption increases with increasing Ni content, and decreases for x from 0.4 to 0.6. This may be because PCP adsorption by $Co_{1-x}Ni_xFe_2O_4$ is primarily physical adsorption, and the adsorption capacity depends mainly on the specific surface area, which corresponds to the tendency of change in the BET surface area shown in Table 1. To guarantee a high adsorption capacity and effective recovery with an external magnetic field, x should preferably be 0.4.

5. Effect of Calcination Temperature

The $Co_{1-x}Ni_xFe_2O_4$/CNTs adsorbent was treated in muffle furnace at different temperatures for 1 h under nitrogen flow. Fig. 8 shows the XRD patterns of $Co_{1-x}Ni_xFe_2O_4$/CNTs treated at different temperatures. No crystalline diffraction peaks appear below 200 °C, which indicates that the $Co_{1-x}Ni_xFe_2O_4$/CNTs nanocomposites are amorphous. At 300 °C, XRD peaks of corresponding to a cubic spinel structure start to appear, which indicates that crystal grains of $Co_{1-x}Ni_xFe_2O_4$ begin to form, but XRD peaks have a weak intensity and significant width, which implies that the crystal grain size is small. At 400 °C, the sample crystalline structure does not change, but the diffraction peaks become sharper with significantly increasing intensity, which indicates that the crystal grains grow gradually and the degree of crystallization increases. The crystal grain size, specific surface area, and saturation magnetization of $Co_{1-x}Ni_xFe_2O_4$ loaded on CNTs are shown in Table 2. The result indicated that as the heat treatment temperature increases, the crystal size increases, the specific surface area decreases, and the saturation magnetization increases. When the specific surface area is large and the crystal grain size is small, the saturation magnetization is low, probably because of the surface and small-size effects of the nanoparticles [31]. The large nanoparticle specific surface area enables more metal ions to reside on the surface of aberrated structures, and the particle surface lattice aberration enables a variation in bond angle and length, which leads to a noncollinearity of the nanoparticle surface magnetic moment, which enables reduced net sample magnetic moment.

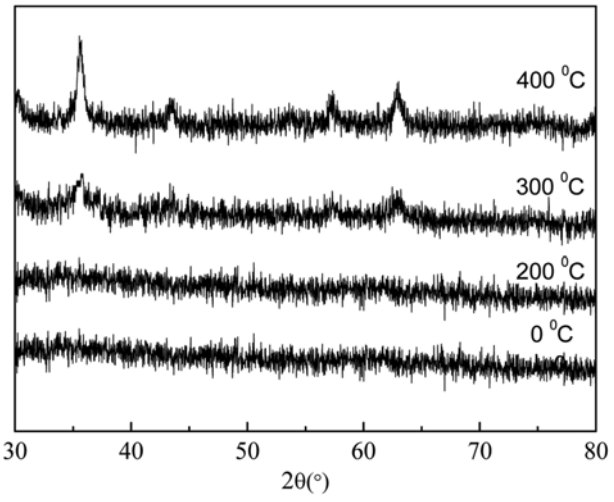

Fig. 8. XRD patterns of $Co_{1-x}Ni_xFe_2O_4$/CNTs treated at different temperatures.

Table 2. Surface structural properties of $Co_{1-x}Ni_xFe_2O_4$/CNTs at different temperatures

Temperature (°C)	Average particle size/ (nm)	Surface area/ ($m^2\ g^{-1}$)	Saturation magnetization/ (emu g^{-1})
100	-	182.2	3.2
200	-	181.9	7.2
300	8	178.5	14.4
400	12	156.5	18.3

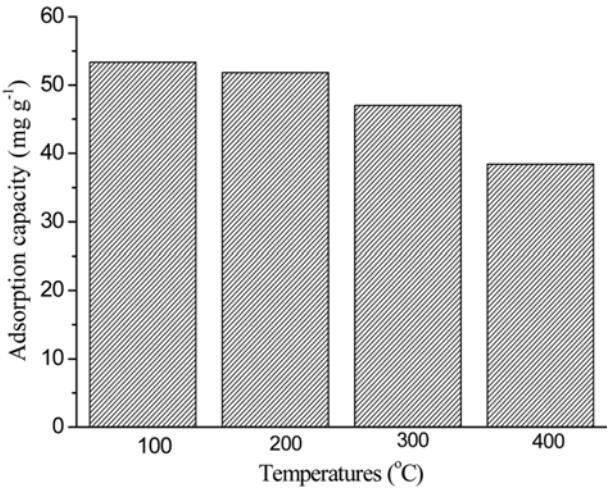

Fig. 9. Effect of treatment temperature on adsorption.

Results for adsorption of PCP by $Co_{1-x}Ni_xFe_2O_4$/CNTs treated at different temperatures are shown in Fig. 9. The result indicated adsorption capacity varies minimally at 100-200 °C, whereas at 200-400 °C, the adsorption capacity obviously reduces with increasing calcination temperature. This is probably because PCP adsorption by $Co_{1-x}Ni_xFe_2O_4$ is primarily physical, and as the calcination temperature increases, the crystal grains grow gradually, whereas the specific surface area decreases, which results in a reduced adsorption capacity. Because of the adsorption capacity and effective magnetic recovery, the preferred calcination temperature is 300 °C.

6. Reuse of Adsorbent

Ferrite magnetic material is a good MW absorbent [32]; thus $Co_{1-x}Ni_xFe_2O_4$/CNTs can be regenerated by MW. In this experiment, a repeated adsorption/MW irradiation regeneration test was designed to investigate the reuse potential of $Co_{1-x}Ni_xFe_2O_4$/CNTs.

After adsorption, 3 g $Co_{1-x}Ni_xFe_2O_4$/CNTs saturated with PCP was placed into a MW regeneration reactor and treated for 3 min at 700 W. The adsorption/MW regeneration was repeated six times. The results are shown in Fig. 10; compared with freshly prepared

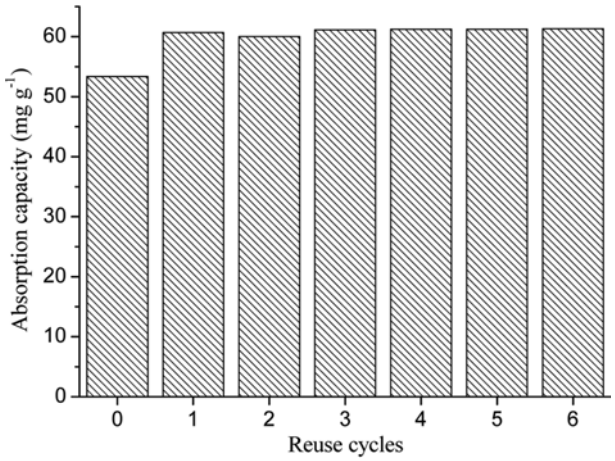

Fig. 10. Absorption capacity of PCP on $Co_{1-x}Ni_xFe_2O_4$/CNTs versus reuse cycles.

$Co_{1-x}Ni_xFe_2O_4$/CNTs, the adsorption capacity increased to 60.0 mg g^{-1} from the second cycle. After that, the adsorption capacity tended to be stable at two to six reuse cycles. The adsorption capacity remained at 60 mg g^{-1} and regeneration efficiency reached 110%.

MW irradiation enables increased crystallinity of loaded $Co_{1-x}Ni_xFe_2O_4$, a larger particle size, and reduced adsorption capacity of $Co_{1-x}Ni_xFe_2O_4$. However, CNTs open and break under MW irradiation, which increases their specific surface area. According to BET analysis, the specific surface area of new $Co_{1-x}Ni_xFe_2O_4$/CNTs was 179.5 m^2 g^{-1}, and after MW regeneration, the specific surface area remained at 185.2 m^2 g^{-1}. During reuse, the adsorbent mass loss is an important economic indicator in actual applications. In this experiment, after six adsorption/regeneration cycles, the mass loss of $Co_{1-x}Ni_xFe_2O_4$/CNTs was 7.3%. Such a mass loss may result from carbonization of some amorphous carbon materials from CNTs or spallation of loaded magnetic material under MW irradiation at elevated temperature.

The results demonstrate that the unique microstructural properties of $Co_{1-x}Ni_xFe_2O_4$/CNTs have strong MW adsorbing capacity, high regeneration efficiency, and high mechanical intensity.

CONCLUSIONS

Magnetically separable $Co_{1-x}Ni_xFe_2O_4$/CNTs adsorbent has been synthesized hydrothermally for efficient removal of PCP from aqueous solution. The $Co_{1-x}Ni_xFe_2O_4$ nanoparticles on CNTs surface showed uniform morphology with small particles. The novel magnetic $Co_{1-x}Ni_xFe_2O_4$/CNTs have excellent adsorption capacity and were used as adsorbent to remove PCP from aqueous solution. The bath adsorption experiments demonstrated that the magnetic property and adsorption capacity of $Co_{1-x}Ni_xFe_2O_4$/CNTs could be controlled through adjusting Ni content and calcination temperature. The optimal Ni content (x) was 0.4 and calcination temperature was 300 °C; at this condition the $Co_{1-x}Ni_xFe_2O_4$/CNTs exhibited the highest adsorption capacity (53.30 mg g^{-1}) and magnetization (14.4 emu g^{-1}). In addition, the saturated $Co_{1-x}Ni_xFe_2O_4$/CNTs can be regenerated efficiently over six cycles. The present work may provide a new approach for the research and development of new adsorbents.

ACKNOWLEDGEMENTS

This work was supported financially by the Nature Science Foundation of China (Nos. 20907025 and 21307065).

REFERENCES

1. Z. H. Jin, C. Yu, X. Y. Wang, Y. Wan, D. Li and G. Z. Lu, *J. Hazard. Mater.*, **186**, 1726 (2011).
2. US Environmental Protection Agency, *National pollutant discharge elimination system*, Code of FederalRe gulations, 40 (1980-1988), Part 122. US Government Printing Office, Washington, DC.
3. K. B. Sanjoy, Y. Qiang and J. Peikang, *J. Hazard. Mater.*, **49**, 143 (1996).
4. Y. C. Sung, J. K. Sook, Y. K. Tae, M. He and J. K. Seung, *Korean J. Chem. Eng.*, **20**, 365 (2003).
5. Z. H. Jin, C. Yu, X. Y. Wang, Y. Wan, D. Li and G. Z. Lu, *J. Hazard. Mater.*, **186**, 1726 (2011).
6. M. Pera-Titus, V. Garcia-Molina, M. A. Banos, J. Gimenez and S. Esplugas, *Appl. Catal. B: Environ.*, **47**, 219 (2004).
7. J. Bandara, J. A. Mielczarski and J. Kiwi, *Appl. Catal. B: Environ.*, **34**, 307 (2001).
8. A. Ghaffari, M. S. Tehrani, S. W. Husain, M. Anbia and P. A. Azar, *J. Nanostruct. Chem.*, **4**, 2 (2014).
9. L. C. Zhou, X. G. Meng, J. W. Fu, Y. C. Yang, P. Yang and Ch. Mi, *Appl. Surf. Sci.*, **292**, 735 (2014).
10. V. K. Gupta, A. Mittal, R. Jain, M. Mathur and S. Sikarwar, J. *Colloid Interface Sci.*, **303**, 80 (2006).
11. X. M. Ren, C. L. Chen, M. Nagatsu and X. K. Wang, *Chem. Eng. J.*, **170**, 395 (2011).
12. X. Yang, J. Lee, L. Yuan, S. R. Chae, V. K. Peterson, A. I. Minett, Y. Yin and A. T. Harris, *Carbon*, **59**, 160 (2013).
13. A. F. Alkaim, Z. Sadik, D. K. Mahdi, S. M. Alshrefi, A. M. Al-Sammarraie, F. M. Alamgir, P. M. Singh and A. M. Aljebore, *Korean J. Chem. Eng.*, **32**, 2456 (2015).
14. B. Jia and L. Gao, *J. Phys. Chem. B*, **111**, 5337 (2007).
15. A. Fraczek-Szczypta, E. Menaszek and S. Blazewicz, *J. Nanomater.*, **13**, 99 (2011).
16. Y. Chang and D. Chen, *J. Colloid Interface Sci.*, **283**, 446 (2005).
17. L. C. A. Oliveira, R. V. R. A. Rios, J. D. Fabris, V. Garg, K. Sapag and R. M. Lago, *Carbon*, **40**, 2177 (2002).
18. M. Abdel Salam, M. A. Gabal and A. Y. Obaid, *Synth. Met.*, **161**, 2651 (2012).
19. V. K. Gupta, S. Agarwal and T. A. Saleh, *Water Res.*, **45**, 2207 (2011).
20. H. Wei, L. Xu, J. Ren and L. Jia, *Colloids Surf., A*, **405**, 38 (2012).
21. H. Y. Zhu, R. Jiang, L. Xiao and G. M. Zeng, *Bioresour. Technol.*, **101**, 5063 (2010).
22. J. L. Gong, B. Wang, G. M. Zeng, C. P. Yang, C. G. Niu, Q. Y. Niu, W. J. Zhou and Y. Liang, *J. Hazard. Mater.*, **164**, 1517 (2009).
23. F. Yu, J. H. Chen, L. Chen, J. Huai, W. Y. Gong, Z. W. Yuan, J. H. Wang and J. Ma, *J. Colloid Interface Sci.*, **378**, 175 (2012).
24. A. A. Farghali, M. Bahgat, W. M. A. El Rouby and M. H. Khedr, *J. Solution Chem.*, **41**, 2209 (2012).
25. C. Y. Cui, X. Quan, H. T. Yu, Y. H. Han and S. Chen, *Appl. Catal.*,

B, **80**, 122 (2008).
26. C. Y. Cui, Q. Z. Zheng, Y. H. Han and Y. J. Xin, *Appl. Surf. Sci.*, **346**, 99 (2015).
27. H. Q. Wu, T. T. Li, L. L. Xia and X. J. Zhang, *Mater. Res. Bull.*, **48**, 4785 (2013).
28. H. X. Li, H. S. Luo and Z. Li, *J. Mol. Catal., A.*, **203**, 267 (2003).
29. F. C. Wu, R. L. Tseng and R. S. Juang, *Water Res.*, **35**, 613 (2001).
30. J. M. Li, X. G. Meng, C. W. Hu and J. Du, *Bioresour. Technol.*, **100**, 1168 (2009).
31. T. J. Lewis, *IEEE Trans. Dielectr. Electr. Insul.*, **11**, 739 (2004).
32. G. Li, L. M. Sheng, L. M. Yu, K. An, W. Ren and X. L. Zhao, *Mater. Sci. Eng. B*, **193**, 153 (2015).